

Comparing Combinations of Linear and Nonlinear Feedback Terms for Motion Control of Marine Surface Vessels

Mikkel Eske Nørgaard Sørensen* Morten Breivik*

**Centre for Autonomous Marine Operations and Systems, Department of Engineering Cybernetics, Norwegian University of Science and Technology (NTNU), NO-7491 Trondheim, Norway
E-mail: mikkels.sorensen@itk.ntnu.no, morten.breivik@ieee.org*

Abstract: Nonlinear control algorithms are often designed with linear feedback terms. Such linear feedback typically gives rise to nice exponential stability properties, but are not physically realistic since all actuators have magnitude constraints. One way to address such constraints can be to introduce nonlinear feedback terms. Hence, this paper investigates combinations of linear and nonlinear feedback terms for pose and velocity control of marine surface vessels. Three cascaded controllers are developed and compared through three simulation scenarios and one model-scale experiment. The comparisons are made using performance metrics which consider both control accuracy and energy use.

Keywords: Marine surface vessel, Cascaded control, Nonlinear feedback control, Target tracking, Constant bearing guidance, Performance metrics

1. INTRODUCTION

Automatic motion control of marine surface vessels has been a research topic since the early 20th century. In recent years, the research has expanded from control of manned vessels to also include unmanned vessels. However, many motion control algorithms found in the literature do not inherently consider physical saturation constraints for the actuators. For example, the nonlinear control algorithms in (Fossen and Strand, 1999), (Fossen, 2000), (Refsnes et al., 2008), (Fossen, 2011) and (Chen et al., 2013) are all designed with linear feedback terms.

This paper therefore investigates combinations of linear and nonlinear feedback terms for pose and velocity control of marine surface vessels. In particular, the nonlinear feedback terms are developed based on constant bearing (CB) guidance principles, inspired by the guided dynamic positioning approach originally suggested in (Breivik et al., 2006). Further inspiration has been found in (Breivik and Fossen, 2007) on the concept of guided motion control, as well as in (Breivik and Fossen, 2009). Also, the concept of CB guided motion control was employed in (Breivik and Loberg, 2011) for a virtual target-based underway docking control system, achieving docking of an unmanned surface vehicle with a mother ship moving in transit at sea. Similarly, a CB guided heading controller was designed in (Skejjic et al., 2011) in order to maneuver a ship around a floating object in deep and calm water under the influence of a uniform current.

Specifically, three cascaded controllers are developed in the paper, where the feedback connection between pose and

velocity which is traditionally found in backstepping control design has been removed. The controllers respectively employ linear feedback for both the pose and velocity control errors (LP-LV), nonlinear feedback for the pose control error and linear feedback for the velocity control error (NP-LV), as well as nonlinear feedback for both the pose and velocity control errors (NP-NV). The performance of the controllers are compared through three simulation scenarios and one model-scale experiment, where the comparisons are made using performance metrics which consider both control accuracy and energy use.

The structure of the paper is as follows: A mathematical vessel model and assumptions are presented in Section 2; Section 3 presents the design of three different cascaded control laws inspired by backstepping and CB guidance; Section 4 includes simulation results, experimental results and a performance evaluation; while Section 5 concludes the paper.

2. MARINE SURFACE VESSEL MODEL

The motion of a surface vessel can be represented by the pose vector $\boldsymbol{\eta} = [x, y, \psi]^T \in \mathbb{R}^2 \times \mathbb{S}$ and the velocity vector $\boldsymbol{\nu} = [u, v, r]^T \in \mathbb{R}^3$, where $\mathbb{S} \in [-\pi, \pi]$. Here, (x, y) represents the Cartesian position in the local earth-fixed reference frame, ψ is the yaw angle, (u, v) represents the body-fixed linear velocities and r is the yaw rate. The 3 degrees-of-freedom dynamics of a surface vessel can then be stated as (Fossen, 2011):

$$\dot{\boldsymbol{\eta}} = \mathbf{R}(\psi)\boldsymbol{\nu} \quad (1)$$

$$\mathbf{M}\dot{\boldsymbol{\nu}} + \mathbf{C}(\boldsymbol{\nu})\boldsymbol{\nu} + \mathbf{D}(\boldsymbol{\nu})\boldsymbol{\nu} = \boldsymbol{\tau}, \quad (2)$$

where

$$\mathbf{R}(\psi) = \begin{bmatrix} \cos(\psi) & -\sin(\psi) & 0 \\ \sin(\psi) & \cos(\psi) & 0 \\ 0 & 0 & 1 \end{bmatrix} \quad (3)$$

is a rotation matrix $\mathbf{R} \in SO(3)$, and where \mathbf{M} , $\mathbf{C}(\boldsymbol{\nu})$, $\mathbf{D}(\boldsymbol{\nu})$ and $\boldsymbol{\tau}$ represent the inertia matrix, Coriolis and centripetal matrix, damping matrix and control input vector, respectively. Here, the system matrices are assumed to satisfy the properties $\mathbf{M} = \mathbf{M}^\top > 0$, $\mathbf{C}(\boldsymbol{\nu}) = -\mathbf{C}(\boldsymbol{\nu})^\top$ and $\mathbf{D}(\boldsymbol{\nu}) > 0$.

Since this paper focuses on fundamental motion control aspects, it is assumed that both the pose vector $\boldsymbol{\eta}$ and velocity vector $\boldsymbol{\nu}$ can be measured, and that no disturbances and uncertainties are affecting the system. Such assumptions will be relaxed and investigated elsewhere.

3. FEEDBACK CONTROL DESIGN

The control objective is to make $\tilde{\boldsymbol{\eta}}(t) \triangleq \boldsymbol{\eta}(t) - \boldsymbol{\eta}_t(t) \rightarrow \mathbf{0}$ as $t \rightarrow \infty$, where $\boldsymbol{\eta}_t(t) = [x_t(t), y_t(t), \psi_t(t)]^\top \in \mathbb{R}^2 \times \mathbb{S}$ represents the pose associated with a target point which is \mathcal{C}^2 and bounded. The motion of the target is typically defined by a human or generated by a guidance system.

The control design is divided into two stages, including definition of new state variables and deriving the control laws through control Lyapunov functions (CLFs). The design is similar to the backstepping method, which has been applied in e.g. (Fossen and Strand, 1999) and (Sørensen and Breivik, 2015), but omits the coupling between the pose and velocity control loops, resulting in a cascade system. This cascade system represents a classical inner-outer loop guidance and control structure, where the outer loop handles the kinematics and the inner loop handles the vessel kinetics. The total system can then be analysed by cascade theory (Lamnabhi-Lagarrigue et al., 2005).

In particular, it is desirable to investigate the effect of using nonlinear feedback terms, inspired by CB guidance (Breivik and Fossen, 2009), compared to standard linear feedback terms. Consequently, we investigate three combinations of linear and nonlinear feedback terms.

For notational simplicity, the time t is omitted in the rest of this section.

3.1 Linear Pose and Velocity Feedbacks

Start by defining the error variables \mathbf{z}_1 and \mathbf{z}_2 :

$$\mathbf{z}_1 \triangleq \mathbf{R}^\top(\psi)(\boldsymbol{\eta} - \boldsymbol{\eta}_t) \quad (4)$$

$$\mathbf{z}_2 \triangleq \boldsymbol{\nu} - \boldsymbol{\alpha}, \quad (5)$$

where $\boldsymbol{\alpha} \in \mathbb{R}^3$ is a vector of stabilising functions, which can be interpreted as a desired velocity and which is to be designed later.

Kinematic Control

Choosing the positive definite CLF

$$V_1 \triangleq \frac{1}{2} \mathbf{z}_1^\top \mathbf{z}_1, \quad (6)$$

the derivative of V_1 with respect to time along the \mathbf{z}_1 -dynamics gives

$$\begin{aligned} \dot{V}_1 &= \mathbf{z}_1^\top \dot{\mathbf{z}}_1 \\ &= \mathbf{z}_1^\top (\mathbf{S}(r)^\top \mathbf{R}^\top(\psi)(\boldsymbol{\eta} - \boldsymbol{\eta}_t) + \mathbf{R}^\top(\psi)(\dot{\boldsymbol{\eta}} - \dot{\boldsymbol{\eta}}_t)) \\ &= \mathbf{z}_1^\top (\mathbf{S}(r)^\top \mathbf{z}_1 + \mathbf{R}^\top(\psi)(\dot{\boldsymbol{\eta}} - \dot{\boldsymbol{\eta}}_t)), \end{aligned} \quad (7)$$

where

$$\mathbf{S}(r) = \begin{bmatrix} 0 & -r & 0 \\ r & 0 & 0 \\ 0 & 0 & 0 \end{bmatrix} \quad (8)$$

is a skew-symmetric matrix satisfying $\mathbf{z}_1^\top \mathbf{S}(r)^\top \mathbf{z}_1 = 0$, which gives

$$\dot{V}_1 = \mathbf{z}_1^\top (\boldsymbol{\nu} - \mathbf{R}^\top(\psi)\dot{\boldsymbol{\eta}}_t). \quad (9)$$

Using (5), the CLF becomes

$$\begin{aligned} \dot{V}_1 &= \mathbf{z}_1^\top (\mathbf{z}_2 + \boldsymbol{\alpha} - \mathbf{R}^\top(\psi)\dot{\boldsymbol{\eta}}_t) \\ &= \mathbf{z}_1^\top \mathbf{z}_2 + \mathbf{z}_1^\top (\boldsymbol{\alpha} - \mathbf{R}^\top(\psi)\dot{\boldsymbol{\eta}}_t), \end{aligned} \quad (10)$$

where the stabilising function can be chosen as

$$\boldsymbol{\alpha} = \mathbf{R}^\top(\psi)\dot{\boldsymbol{\eta}}_t - \mathbf{K}_1 \mathbf{z}_1 \quad (11)$$

with $\mathbf{K}_1 > 0$, which results in

$$\dot{V}_1 = -\mathbf{z}_1^\top \mathbf{K}_1 \mathbf{z}_1 + \mathbf{z}_1^\top \mathbf{z}_2. \quad (12)$$

It can be concluded that the origin of \mathbf{z}_1 is uniformly globally exponentially stable (UGES) when seeing \mathbf{z}_2 as an input with $\mathbf{z}_2 = \mathbf{0}$. Consequently, it can be concluded by Lemma 4.6 from (Khalil, 2002) that the subsystem

$$\dot{\mathbf{z}}_1 = \mathbf{S}(r)^\top \mathbf{z}_1 - \mathbf{K}_1 \mathbf{z}_1 + \mathbf{z}_2 \quad (13)$$

is input-to-state stable (ISS). Note that (12) shows that $\mathbf{S}(r)$ in (13) does not affect the ISS property.

Kinetic Control

The \mathbf{z}_2 -dynamics can be written as

$$\begin{aligned} \mathbf{M}\dot{\mathbf{z}}_2 &= \mathbf{M}(\dot{\boldsymbol{\nu}} - \dot{\boldsymbol{\alpha}}) \\ &= \boldsymbol{\tau} - \mathbf{C}(\boldsymbol{\nu})\boldsymbol{\nu} - \mathbf{D}(\boldsymbol{\nu})\boldsymbol{\nu} - \mathbf{M}\dot{\boldsymbol{\alpha}}, \end{aligned} \quad (14)$$

where the time derivative of (11) becomes

$$\dot{\boldsymbol{\alpha}} = \mathbf{R}^\top(\psi)\dot{\boldsymbol{\eta}}_t + \mathbf{S}(r)^\top \mathbf{R}^\top(\psi)\dot{\boldsymbol{\eta}}_t - \mathbf{K}_1 \dot{\mathbf{z}}_1 \quad (15)$$

where $\boldsymbol{\eta}_t$ is the pose of the target point and $\dot{\mathbf{z}}_1$ given by (13). The CLF for \mathbf{z}_2 is then defined as

$$V_2 \triangleq \frac{1}{2} \mathbf{z}_2^\top \mathbf{M} \mathbf{z}_2. \quad (16)$$

Simplifying $\mathbf{C}(\boldsymbol{\nu}) = \mathbf{C}$, $\mathbf{D}(\boldsymbol{\nu}) = \mathbf{D}$, $\mathbf{R}(\psi) = \mathbf{R}$ and $\mathbf{S}(r) = \mathbf{S}$ for notational brevity, the derivative of (16) becomes

$$\begin{aligned} \dot{V}_2 &= \mathbf{z}_2^\top \mathbf{M} \dot{\mathbf{z}}_2 \\ &= \mathbf{z}_2^\top (\boldsymbol{\tau} - \mathbf{C}\boldsymbol{\nu} - \mathbf{D}\boldsymbol{\nu} - \mathbf{M}\dot{\boldsymbol{\alpha}}). \end{aligned} \quad (17)$$

The control input can be chosen as

$$\boldsymbol{\tau} = \mathbf{M}\dot{\boldsymbol{\alpha}} + \mathbf{C}\boldsymbol{\nu} + \mathbf{D}\boldsymbol{\nu} - \mathbf{K}_2 \mathbf{z}_2, \quad (18)$$

where $\mathbf{K}_2 > 0$, which results in

$$\dot{V}_2 = -\mathbf{z}_2^\top \mathbf{K}_2 \mathbf{z}_2 < 0, \quad (19)$$

which makes the origin of the \mathbf{z}_2 -dynamics

$$\dot{\mathbf{z}}_2 = -\mathbf{M}^{-1} \mathbf{K}_2 \mathbf{z}_2 \quad (20)$$

UGES.

It should be noted that it is possible to choose $\boldsymbol{\tau}$ in (18) as e.g.

$$\boldsymbol{\tau} = \mathbf{M}\dot{\boldsymbol{\alpha}} + \mathbf{C}\boldsymbol{\alpha} + \mathbf{D}\boldsymbol{\alpha} - \mathbf{K}_2 \mathbf{z}_2, \quad (21)$$

but this choice is not desirable since it changes (20) to

$$\dot{\mathbf{z}}_2 = -\mathbf{M}^{-1}(\mathbf{C} + \mathbf{D} + \mathbf{K}_2)\mathbf{z}_2, \quad (22)$$

where the convergence rate of the \mathbf{z}_2 -dynamics becomes influenced by the vessel \mathbf{C} and \mathbf{D} matrices.

Stability Analysis

The total closed-loop dynamics become

$$\dot{\mathbf{z}}_1 = \mathbf{S}^\top \mathbf{z}_1 - \mathbf{K}_1 \mathbf{z}_1 + \mathbf{z}_2 \quad (23)$$

$$\dot{\mathbf{z}}_2 = -\mathbf{M}^{-1} \mathbf{K}_2 \mathbf{z}_2. \quad (24)$$

Since the origins of both subsystems are UGES if the \mathbf{z}_1 -dynamics in (23) is unperturbed ($\mathbf{z}_2 = \mathbf{0}$), and the kinematic control loop has linear growth in the perturbation term \mathbf{z}_2 , all the conditions of Theorem 2.1 and Proposition 2.3 from (Lamnabhi-Lagarrigue et al., 2005) are satisfied, and therefore the origin of the overall system $(\mathbf{z}_1, \mathbf{z}_2) = (\mathbf{0}, \mathbf{0})$ is UGES.

3.2 Nonlinear Pose Feedback and Linear Velocity Feedback

We now introduce nonlinear pose feedback inspired by constant bearing (CB) guidance, which was originally used for vessel control in (Breivik et al., 2006). CB guidance is a so-called two-point guidance scheme developed for interceptor missiles, where the interceptor is supposed to align the relative interceptor-target velocity along the line-of-sight (LOS) vector between the interceptor and the target.

The most common method of implementing CB guidance is to make the rotation rate of the interceptor velocity directly proportional to the rotation rate of the interceptor-target LOS, which is widely known as proportional navigation. However, CB guidance can also be implemented through the direct velocity assignment

$$\mathbf{v}_d = \mathbf{v}_t - \kappa \frac{\tilde{\mathbf{p}}}{\|\tilde{\mathbf{p}}\|}, \quad (25)$$

where $\mathbf{v}_t \in \mathbb{R}^2$ is the target velocity and

$$\tilde{\mathbf{p}} \triangleq \mathbf{p} - \mathbf{p}_t \quad (26)$$

is the LOS vector between the interceptor position $\mathbf{p} = [x, y]^\top$ and the target position $\mathbf{p}_t = [x_t, y_t]^\top$, such that

$$\|\tilde{\mathbf{p}}\| \triangleq \sqrt{\tilde{\mathbf{p}}^\top \tilde{\mathbf{p}}} \geq 0, \quad (27)$$

is the Euclidean length of $\tilde{\mathbf{p}}$. Additionally, $\kappa \geq 0$, which can be chosen as

$$\kappa = U_{a,max} \frac{\|\tilde{\mathbf{p}}\|}{\sqrt{\tilde{\mathbf{p}}^\top \tilde{\mathbf{p}} + \Delta_{\tilde{\mathbf{p}}}^2}}, \quad (28)$$

where $U_{a,max} > 0$ represents the maximum approach speed toward the target and $\Delta_{\tilde{\mathbf{p}}} > 0$ is a tuning parameter which affects the transient convergence behavior between the interceptor and target. The concept of using such nonlinear feedback is shown in Fig. 1.

By introducing nonlinear feedback based on CB guidance to the controller, the stabilising function can now be chosen as

$$\boldsymbol{\alpha} = \mathbf{R}^\top \dot{\boldsymbol{\eta}}_t - \mathbf{K}_1(\mathbf{z}_1, \Delta_i) \mathbf{z}_1, \quad (29)$$

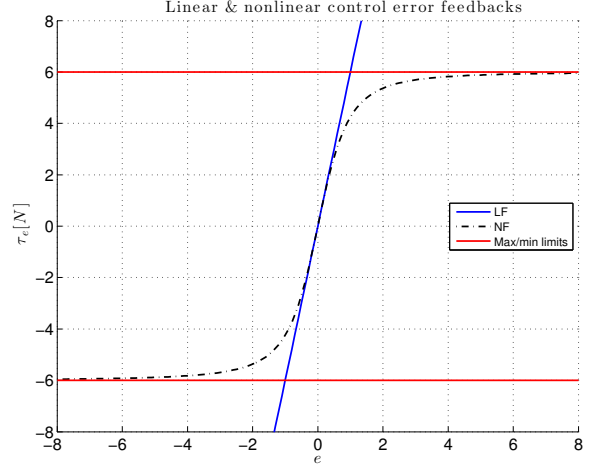


Fig. 1. LF is a linear feedback term as a function of the control error e , while NF is a nonlinear feedback term based on a sigmoid function of e

where

$$\mathbf{K}_1(\mathbf{z}_1, \Delta_i) = \mathbf{K}_1 \begin{bmatrix} \frac{1}{\sqrt{\mathbf{z}_{1,\tilde{\mathbf{p}}}^\top \mathbf{z}_{1,\tilde{\mathbf{p}}} + \Delta_{\tilde{\mathbf{p}}}^2}} \mathbf{I}_{2 \times 2} & \mathbf{0}_{2 \times 1} \\ \mathbf{0}_{1 \times 2} & \frac{1}{\sqrt{z_{1,\tilde{\psi}}^2 + \Delta_{\tilde{\psi}}^2}} \end{bmatrix} \quad (30)$$

and $\mathbf{K}_1 > 0$ as before, $\mathbf{z}_{1,\tilde{\mathbf{p}}} \triangleq [z_{1,1}, z_{1,2}]^\top$, $z_{1,\tilde{\psi}} \triangleq z_{1,3}$, $\Delta_{\tilde{\mathbf{p}}} > 0$ and $\Delta_{\tilde{\psi}} > 0$. However, it is also possible to choose

$$\mathbf{K}_1(\mathbf{z}_1, \Delta_i) = \mathbf{K}_1 \begin{bmatrix} \frac{1}{\sqrt{\mathbf{z}_1^\top \mathbf{z}_1 + \Delta^2}} \mathbf{I}_{3 \times 3} \end{bmatrix}, \quad (31)$$

if $\Delta_{\tilde{\mathbf{p}}} = \Delta_{\tilde{\psi}} = \Delta > 0$, but then it is not possible to define a different transient behavior for the position and heading.

Choosing (30) leads to

$$\dot{\boldsymbol{\alpha}} = \mathbf{R}^\top \dot{\boldsymbol{\eta}}_t + \mathbf{S}^\top \mathbf{R}^\top \dot{\boldsymbol{\eta}}_t - \dot{\mathbf{K}}_1(\mathbf{z}_1, \Delta_i) \mathbf{z}_1 - \mathbf{K}_1(\mathbf{z}_1, \Delta_i) \dot{\mathbf{z}}_1, \quad (32)$$

where

$$\dot{\mathbf{K}}_1(\mathbf{z}_1, \Delta_i) = -\mathbf{K}_1 \begin{bmatrix} \frac{\mathbf{z}_{1,\tilde{\mathbf{p}}}^\top \dot{\mathbf{z}}_{1,\tilde{\mathbf{p}}} \mathbf{I}_{2 \times 2}}{(\mathbf{z}_{1,\tilde{\mathbf{p}}}^\top \mathbf{z}_{1,\tilde{\mathbf{p}}} + \Delta_{\tilde{\mathbf{p}}}^2)^{\frac{3}{2}}} & \mathbf{0}_{2 \times 1} \\ \mathbf{0}_{1 \times 2} & \frac{z_{1,\tilde{\psi}} \dot{z}_{1,\tilde{\psi}}}{(z_{1,\tilde{\psi}}^2 + \Delta_{\tilde{\psi}}^2)^{\frac{3}{2}}} \end{bmatrix}. \quad (33)$$

Stability Analysis

The total closed-loop dynamics now changes to

$$\dot{\mathbf{z}}_1 = \mathbf{S}^\top \mathbf{z}_1 - \mathbf{K}_1(\mathbf{z}_1, \Delta_i) \mathbf{z}_1 + \mathbf{z}_2 \quad (34)$$

$$\dot{\mathbf{z}}_2 = -\mathbf{M}^{-1} \mathbf{K}_2 \mathbf{z}_2. \quad (35)$$

Here, we can see that

$$\|\mathbf{z}_1\| \gg 1 \Rightarrow \dot{\mathbf{z}}_1 = \mathbf{S}^\top \mathbf{z}_1 - \mathbf{K}_1 + \mathbf{z}_2 \quad (36)$$

and

$$\|\mathbf{z}_1\| \approx 0 \Rightarrow \dot{\mathbf{z}}_1 = \mathbf{S}^\top \mathbf{z}_1 - \mathbf{K}_1 \begin{bmatrix} \frac{1}{\Delta_{\tilde{\mathbf{p}}}} \mathbf{I}_{2 \times 2} & \mathbf{0}_{2 \times 1} \\ \mathbf{0}_{1 \times 2} & \frac{1}{\Delta_{\tilde{\psi}}} \end{bmatrix} \mathbf{z}_1 + \mathbf{z}_2. \quad (37)$$

Hence, by introducing nonlinear pose feedback, the stability of the origin of the unperturbed \mathbf{z}_1 subsystem is changed to uniform semiglobal exponential stability (USGES), since the values Δ_i in (30) can be chosen arbitrarily large, see also Theorem 1 in (Fossen and Pettersen, 2014). This also changes the stability of the origin of the total system to USGES.

3.3 Nonlinear Pose and Velocity Feedbacks

We now also introduce nonlinear velocity feedback, which changes the control law (18) to

$$\boldsymbol{\tau} = \mathbf{M}\dot{\boldsymbol{\alpha}} + \mathbf{C}\boldsymbol{\nu} + \mathbf{D}\boldsymbol{\nu} - \mathbf{K}_2(\mathbf{z}_2, \Delta_i)\mathbf{z}_2, \quad (38)$$

where

$$\mathbf{K}_2(\mathbf{z}_2, \Delta_i) = \mathbf{K}_2 \begin{bmatrix} 1 & \mathbf{0}_{2 \times 1} \\ \frac{1}{\sqrt{\mathbf{z}_{2,\bar{v}}^\top \mathbf{z}_{2,\bar{v}} + \Delta_{\bar{v}}^2}} \mathbf{I}_{2 \times 2} & \\ \mathbf{0}_{1 \times 2} & \frac{1}{\sqrt{z_{2,\bar{r}}^2 + \Delta_{\bar{r}}^2}} \end{bmatrix} \quad (39)$$

with $\mathbf{K}_2 > 0$ as before, and where $\mathbf{z}_{2,\bar{v}}$ and $z_{2,\bar{r}}$ are defined as $\mathbf{z}_{2,\bar{v}} \triangleq [z_{2,1}, z_{2,2}]^\top$, $z_{2,\bar{r}} \triangleq z_{2,3}$, $\Delta_{\bar{v}} > 0$ and $\Delta_{\bar{r}} > 0$.

Stability Analysis

The total closed-loop dynamics become

$$\dot{\mathbf{z}}_1 = \mathbf{S}^\top \mathbf{z}_1 - \mathbf{K}_1(\mathbf{z}_1, \Delta_i)\mathbf{z}_1 + \mathbf{z}_2 \quad (40)$$

$$\dot{\mathbf{z}}_2 = -\mathbf{M}^{-1}\mathbf{K}_2(\mathbf{z}_2, \Delta_i)\mathbf{z}_2. \quad (41)$$

The stability of the origin of the \mathbf{z}_2 subsystem is now also changed to USGES, and utilizing Theorem 2.1 and Proposition 2.3 from (Lamnabhi-Lagarrigue et al., 2005), it can be concluded that the origin of the total system is USGES.

4. SIMULATION AND EXPERIMENTAL RESULTS

The model-scale ship Cybership Enterprise I, with parameters from (Sandved, 2015), will be used to test the performance of the proposed motion controllers through both numerical simulations in Matlab and model-scale experiments in an ocean basin. Cybership Enterprise I is a 1:70 scale replica of a supply ship, with a length of $L = 1.105$ (m). It is fully actuated with two Voith-Schneider propellers aft and one bow thruster. We have limited the output of the actuators such that they can only produce a maximum of 2.0 (N) in surge and sway and 1.5 (Nm) in yaw. Hence, the commanded control input with saturation $\boldsymbol{\tau}_s$ is bounded as follows

$$\tau_{s,i}(\tau_i) = \begin{cases} \tau_{i,min} & \text{if } \tau_i \leq \tau_{i,min} \\ \tau_i & \text{if } \tau_{i,min} < \tau_i < \tau_{i,max} \\ \tau_{i,max} & \text{if } \tau_i \geq \tau_{i,max} \end{cases}, \quad \forall i \in \{1, 2, 3\} \quad (42)$$

where $\boldsymbol{\tau}$ is the commanded control input without saturation, such as in (18) and (38), while $\boldsymbol{\tau}_{min} = [\tau_{1,min}, \tau_{2,min}, \tau_{3,min}]^\top$ with negative and bounded elements and $\boldsymbol{\tau}_{max} = [\tau_{1,max}, \tau_{2,max}, \tau_{3,max}]^\top$ with positive and bounded elements, which represent the magnitude saturation limits. Details about the ship are given in (Sandved, 2015). The experiment is conducted in the Marine Cybernetics Laboratory (MCLab) at NTNU, where it is possible to get

accurate pose measurement through a Qualisys motion capture system.

In this section, the abbreviation LP-LV refers to linear feedback for both the pose and velocity control errors, NP-LV refers to nonlinear feedback for the pose control error and linear feedback for the velocity control error, while NP-NV refers to nonlinear feedback for both the pose and velocity control errors.

Performance Metrics

To evaluate and compare the performance of the different controllers, some performance metrics must be used.

For this, we will use the norm of the pose error e , which can be calculated by

$$e(t) \triangleq \sqrt{\tilde{\boldsymbol{\eta}}(t)^\top \tilde{\boldsymbol{\eta}}(t)}. \quad (43)$$

The performance metric IAE (integral of the absolute error) is then

$$IAE(t) \triangleq \int_0^t |e(\tau)| d\tau, \quad (44)$$

which simply integrates the temporal evolution of the absolute value of the error without adding any weight to the error. We will also use the integral of the absolute error multiplied by the energy consumption (IAEW), which was proposed earlier in (Sørensen and Breivik, 2015). The IAEW can be computed as

$$IAEW(t) \triangleq \int_0^t |e(\tau)| d\tau \int_0^t P(\tau) d\tau, \quad (45)$$

where

$$P(t) = |\boldsymbol{\nu}(t)^\top \boldsymbol{\tau}(t)| \quad (46)$$

represents the mechanical power. IAEW thus indicates which controller has the best combined control accuracy and energy use through one single metric.

4.1 Simulation Results for Straight-Line Motion Control

For a straight-line target motion, the target pose $\boldsymbol{\eta}_t(t)$ is derived from

$$\boldsymbol{\eta}_t(t) = [x_t(t), y_t(t), \psi_t]^\top, \quad (47)$$

where

$$x_t(t) = 1 + v_t t \cos(\psi_t) \quad (48)$$

$$\dot{x}_t(t) = v_t \cos(\psi_t), \quad (49)$$

and

$$y_t(t) = v_t t \sin(\psi_t) \quad (50)$$

$$\dot{y}_t(t) = v_t \sin(\psi_t), \quad (51)$$

where ψ_t is a constant.

The reference target has a constant speed $v_t = 0.15$ (m/s) and $\dot{v}_t = 0$. Hence, the acceleration of the target point is $\ddot{x}_t(t) = 0$ and $\ddot{y}_t(t) = 0$. For the full-scale vessel, this corresponds to 1.275 m/s using the Bis scale (Fossen, 2011). Also, the straight-line trajectory has a constant orientation relative to the x-axis $\psi_t = 0.9273$ (rad), which is equivalent to 53 (deg).

The initial condition of the target pose is chosen to be $\boldsymbol{\eta}_t(0) = [1$ (m), 0 (m), 0.9273 (rad)] $^\top$ and $\dot{\boldsymbol{\eta}}_t(0) = [0.09$

$(m/s), 0.12 (m/s), 0 (rad/s)]^\top$.

In the following, we consider three simulation scenarios to compare and evaluate the different controllers.

Scenario 1: Non-Saturated Control Inputs

The initial vessel states are chosen to be $\boldsymbol{\eta}(0) = [0.5 (m), 0 (m), \pi/8 (rad)]^\top$ and $\boldsymbol{\nu}(0) = [0 (m/s), 0 (m/s), 0 (rad/s)]^\top$, which leads to $\|\mathbf{z}_1(0)\| = 0.7320$, $\|\mathbf{z}_2(0)\| = 0.1961$ for LP-LV and $\|\mathbf{z}_2(0)\| = 0.2262$ for NP-LV and NP-NV. Notice that $\boldsymbol{\alpha}$ is changed when nonlinear feedback terms are introduced, which also affects $\|\mathbf{z}_2(0)\|$. The normed pose error starts at $e(0) = 0.7320$. The constant gain matrices \mathbf{K}_1 and \mathbf{K}_2 are chosen such that the LP-LV controller does not saturate, and hence neither the NP-LV nor NP-NV controllers, see Table 1.

	LP-LV	NP-LV	NP-NV
\mathbf{K}_1	$diag([0.13, 0.13, 0.01])$	- - -	- - -
\mathbf{K}_2	$diag([7, 8, 6])$	- - -	- - -
$\Delta_{\tilde{p}, \tilde{\psi}}$	-	$[0.4, 0.2]$	$[0.4, 0.2]$
$\Delta_{\tilde{v}, \tilde{r}}$	-	-	$[0.97, 0.2]$

Table 1. Control gains for scenarios 1 and 2

In Fig. 2, the vessel and target pose outlines are plotted to show the transient convergence behavior. Here, the blue outline represents the LP-LV-controlled vessel, the dash-dotted black outline represents the NP-LV-controlled vessel, the dashed green outline represents the NP-NV-controlled vessel, while the red outline represents the target.

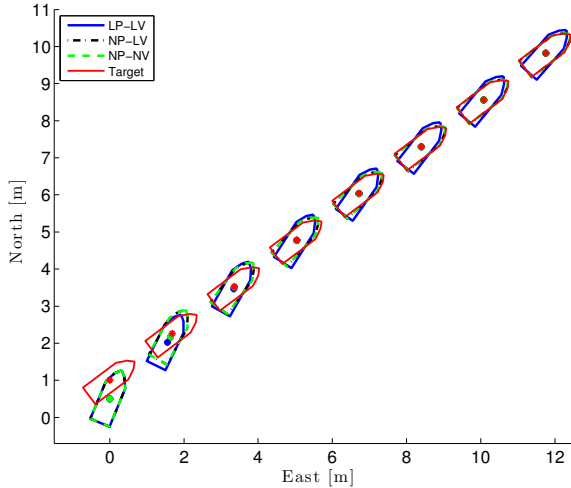


Fig. 2. Scenario 1: The vessel tracking the target moving in a straight-line motion

Fig. 3a illustrates the normed pose error e scaled by the vessel length L , showing that all the controllers are able to track the target. It is worth noting that the introduction of nonlinear feedback control terms lead to significantly faster convergence despite identical gain matrices \mathbf{K}_1 and \mathbf{K}_2 for all the controllers.

The phase-portrait relation between the normed error variables \mathbf{z}_1 and \mathbf{z}_2 is shown in Fig. 3b. Here, we can see that the controllers with nonlinear feedback terms are able to reduce the initial increase in \mathbf{z}_1 faster than the pure linear feedback controller, and achieve a sharper trajectory toward the origin of the \mathbf{z} -dynamics.

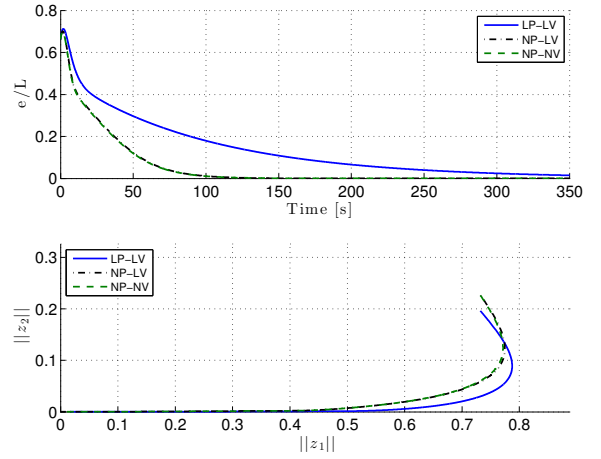


Fig. 3. Scenario 1: The normed pose error scaled by the vessel length (top) and the phase portrait of the normed \mathbf{z} -dynamics (bottom)

The commanded control inputs in Fig. 4 show that all the controllers stay below the saturation limits of 2.0 (N) in surge and sway and 1.5 (Nm) in yaw, which was the criterion when choosing the gain matrices \mathbf{K}_1 and \mathbf{K}_2 .

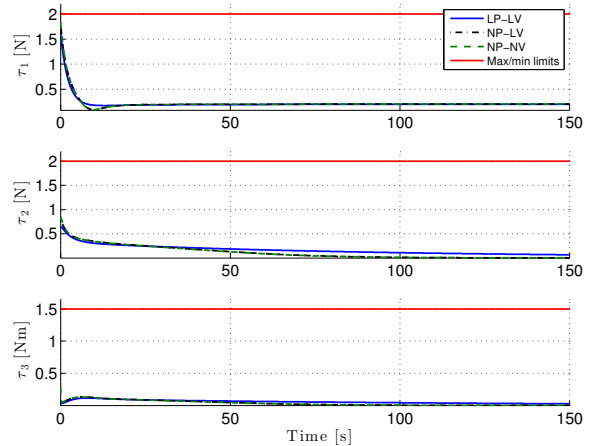


Fig. 4. Scenario 1: The commanded control inputs and force/moment saturation limits

Fig. 5 shows the performance metrics IAE and IAEW for Scenario 1. In particular, Fig. 5a confirms the fact that the nonlinear feedback controllers have the fastest transient response since they quickly establish the smallest IAE value. In addition, Fig. 5b shows that these controllers have the significantly smallest value for combined control accuracy and energy use, thus achieving the best overall control performance for this scenario.

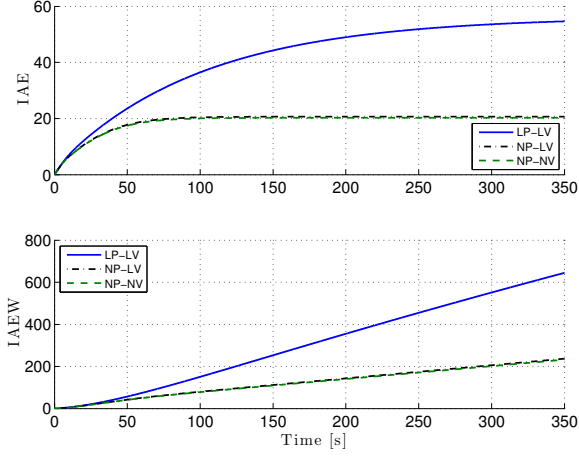


Fig. 5. Scenario 1: IAE and IAEW performance metrics

Scenario 2: Large Initial Errors

By increasing the initial pose error, we can see how sensitive the controllers are to variations in this error. For this scenario, the initial pose of the vessel is therefore changed to $\boldsymbol{\eta}(0) = [-3 \text{ (m)}, -1.4 \text{ (m)}, 0.6\pi \text{ (rad)}]^\top$, which changes the initial errors to $e(0) = 4.3448$, $\|\mathbf{z}_1(0)\| = 4.3448$, $\|\mathbf{z}_2(0)\| = 0.6807$ for LP-LV and $\|\mathbf{z}_2(0)\| = 0.2675$ for NP-LV and NP-NV. The control gains remain unchanged, as in Table 1.

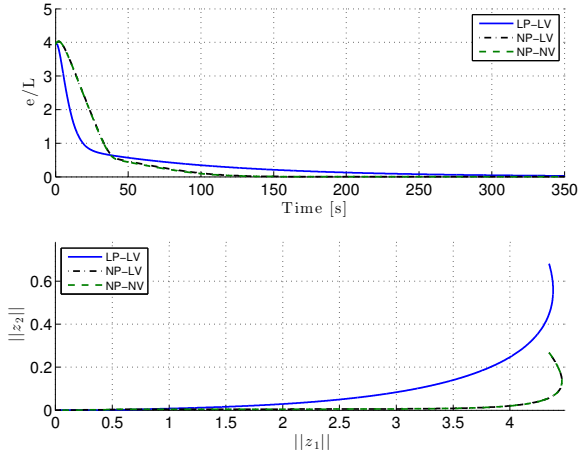


Fig. 6. Scenario 2: The normed pose error scaled by the vessel length (top) and the phase portrait of the normed \mathbf{z} -dynamics (bottom)

Fig. 6a shows that the LP-LV-controlled vessel has the fastest convergence of the normed pose error until about 40 s. However, as seen in Fig. 7, this can be explained by the fact that the LP-LV controller significantly exceeds the saturation limits, which makes it more sensitive to changes in the control errors than its nonlinear counterparts. Fig. 8 is particularly interesting since the IAEW metric shows that the nonlinear feedback controllers achieve a smaller value even from the start, thus achieving the best overall control performance also for this scenario, while staying within the saturation bounds.

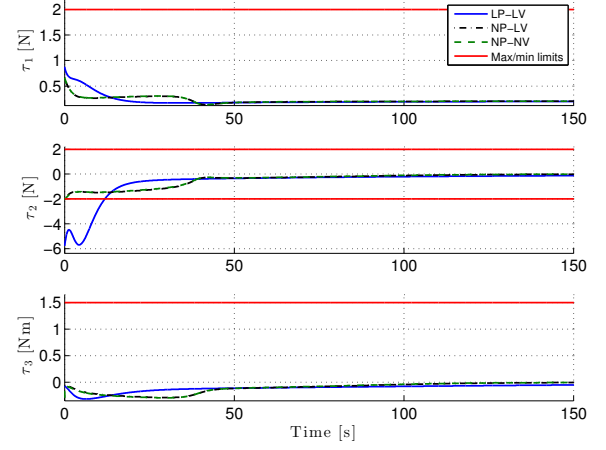


Fig. 7. Scenario 2: The commanded control inputs and force/moment saturation limits

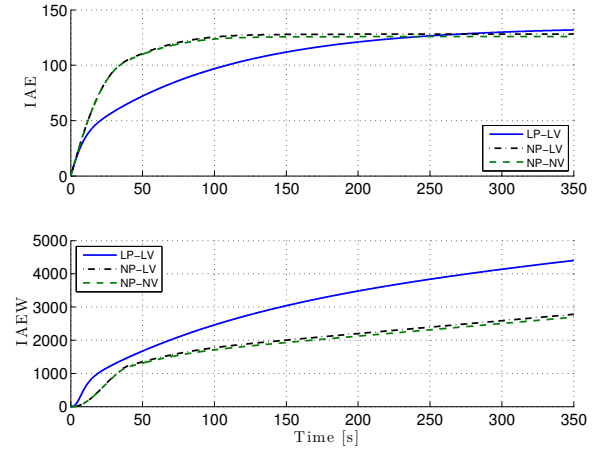


Fig. 8. Scenario 2: IAE and IAEW performance metrics

Scenario 3: Adjusted Nonlinear Gain Parameters

The control parameter Δ is usually known as the lookahead distance in LOS-based control (Breivik and Fossen, 2009). In (Pavlov et al., 2009) it is shown that a small Δ -value corresponds to fast convergence to the path, but with a large overshoot. At the same time, a large Δ -value reduces overshoot and results in smooth but slow convergence. In this scenario, we will investigate the effects of changing the Δ_i parameters for the nonlinear feedback controllers. The initial pose of the vessel is the same as in Scenario 1, with $\boldsymbol{\eta}(0) = [0.5 \text{ (m)}, 0 \text{ (m)}, \pi/8 \text{ (rad)}]^\top$, which means that the initial errors become $e(0) = 0.7320$, $\|\mathbf{z}_1(0)\| = 0.7320$, $\|\mathbf{z}_2(0)\| = 0.1961$ for LP-LV and $\|\mathbf{z}_2(0)\| = 0.2305$ for NP-LV and NP-NV. The updated control gains can be seen in Table 2.

	LP-LV	NP-LV	NP-NV
\mathbf{K}_1	$diag([0.13, 0.13, 0.01])$	- -	- -
\mathbf{K}_2	$diag([7, 8, 6])$	- -	- -
$\Delta_{\tilde{p}, \tilde{\psi}}$	-	$[0.35, 0.01]$	$[0.4, 0.2]$
$\Delta_{\tilde{v}, \tilde{r}}$	-	-	$[0.8, 0.02]$

Table 2. Control gains for Scenario 3

Comparing tables 1 and 2, the parameters $\Delta_{\tilde{p}}$ and $\Delta_{\tilde{\psi}}$ have been decreased for the NP-LV controller, which means that

the region of exponential convergence is decreased. This can be seen in Fig. 9a where the convergence behavior becomes almost discontinuous, which would be unrealistic for a vessel with actuator rate constraints. By not changing the $\Delta_{\tilde{p}, \tilde{\psi}}$ parameters and decreasing the $\Delta_{\tilde{v}, \tilde{r}}$ parameters for the NP-NV controller, Fig. 10 shows a slight violation of the saturation limit of τ_1 . However, both nonlinear feedback controllers continue to perform significantly better than their linear counterpart, as shown in Fig. 11.

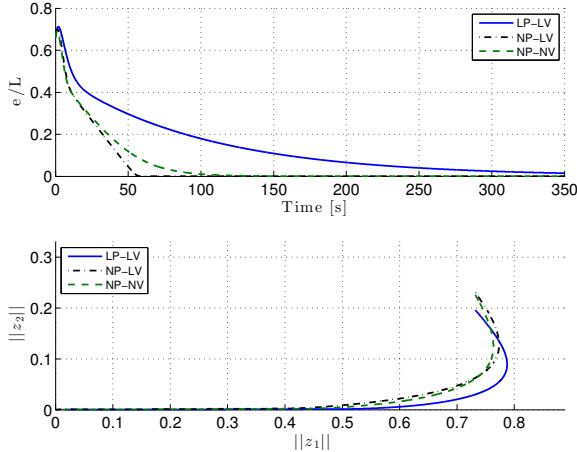


Fig. 9. Scenario 3: The normed pose error scaled by the vessel length (top) and the phase portrait of the normed \mathbf{z} -dynamics (bottom)

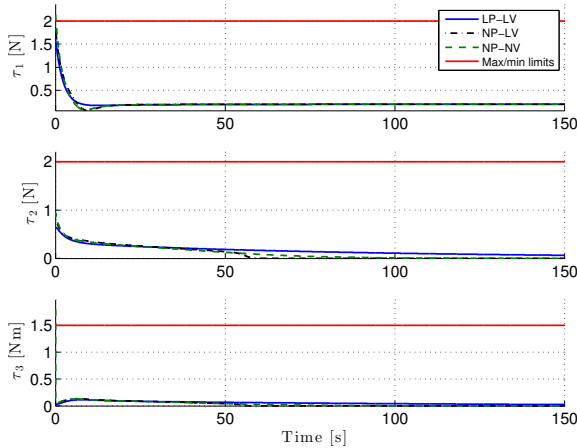


Fig. 10. Scenario 3: The commanded control inputs and force/moment saturation limits

4.2 Experimental Result for Point Stabilisation

The LP-LV and NP-NV controllers have been implemented and experimentally tested for the model-scale ship CyberShip Enterprise I in the Marine Cybernetics Laboratory at NTNU, for a scenario concerning point stabilisation toward a stationary target, where the initial vessel states are $\boldsymbol{\eta}(0) = [0 \text{ (m)}, 0 \text{ (m)}, 0 \text{ (rad)}]^\top$ and $\boldsymbol{\nu}(0) = [0 \text{ (m/s)}, 0 \text{ (m/s)}, 0 \text{ (rad/s)}]^\top$, while the initial target pose is $\boldsymbol{\eta}_t(0) = [2 \text{ (m)}, 2 \text{ (m)}, 1.6 \text{ (rad)}]^\top$. The control parameters are given in Table 3.

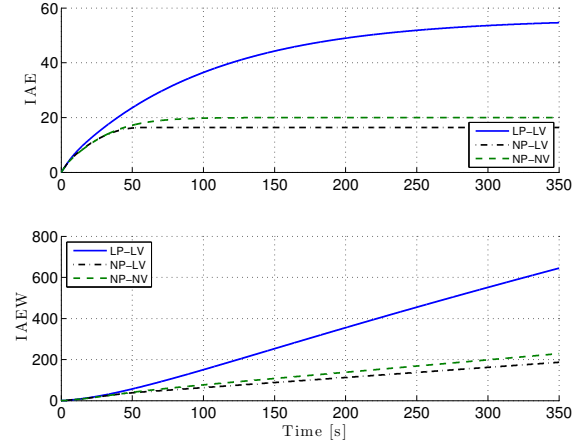


Fig. 11. Scenario 3: IAE and IAEW performance metrics

	LP-LV	NP-NV
\mathbf{K}_1	$\text{diag}([0.2, 0.2, 0.04])$	- -
\mathbf{K}_2	$\text{diag}([7, 8, 6])$	- -
$\Delta_{\tilde{p}, \tilde{\psi}}$	-	$[0.4, 0.2]$
$\Delta_{\tilde{v}, \tilde{r}}$	-	$[0.97, 0.9]$

Table 3. Control gains for the experiment

Fig. 12 shows the transient convergence behavior of the LP-LV-controlled vessel outlined in blue, and the NP-NV-controlled vessel outlined in dashed green, where the dots indicate the final position. For easier viewing, the size of the plotted vessel outline has been made smaller than the real one. As can be seen, the nonlinear feedback controller gives a smooth and energy-efficient motion toward the target, while its linear counterpart moves almost sideways in the beginning, only changing heading toward the end. The final steady-state error is due to a poorly designed control allocation, which means that the actual output from the actuators is zero even though the controllers command a non-zero output, which can be seen in Fig. 13. This figure also shows that the LP-LV controller's commands exceed the saturation limits in the beginning, resulting in a rapid-as-possible convergence toward the target, which can also be observed through the IAE metric in Fig. 14a. However, the NP-NV controller still has the best overall performance as shown by the IAEW metric in Fig. 14b, and the NP-NV-controlled ship is seen to be located closer to the target at the end.

5. CONCLUSION

This paper has investigated combinations of linear and nonlinear feedback terms for pose and velocity control of marine surface vessels. Three cascaded controllers were developed and compared through numerical simulations and a model-scale experiment. Two performance metrics were used to compare the behavior of the controllers. Interestingly, the nonlinear feedback controllers outperformed their linear counterpart in all scenarios, concerning both the handling of actuator saturation limits and the combined performance of control accuracy and energy use. Another lesson is that the nonlinear gain parameters should not be chosen too small. Future work includes introducing model uncertainties and unknown disturbances to the vessel system. It is also relevant to consider actuator

ACKNOWLEDGEMENTS

This work was supported by the Research Council of Norway through the Centres of Excellence funding scheme, project number 223254.

REFERENCES

- Breivik, M. and Fossen, T.I. (2007). Applying missile guidance concepts to motion control of marine craft. *in Proceedings of the 7th IFAC Conference on Control Applications in Marine Systems, Bol, Croatia*.
- Breivik, M. and Fossen, T.I. (2009). *Guidance laws for autonomous underwater vehicles*. in A. V. Inzartsev, *Underwater Vehicles*, IN-TECH Education and Publishing, 51-76.
- Breivik, M. and Loberg, J.E. (2011). A virtual target-based under-way docking procedure for unmanned surface vehicles. *in Proceedings of the 18th IFAC World Congress, Milano, Italy*.
- Breivik, M., Strand, J.P., and Fossen, T.I. (2006). Guided dynamic positioning for fully actuated marine surface vessels. *in Proceedings of the 7th IFAC Conference on Manoeuvring and Control of Marine Craft, Lisbon, Portugal*.
- Chen, M., Ge, S., How, B., and Choo, Y. (2013). Robust adaptive position mooring control for marine vessels. *IEEE Transactions on Control Systems Technology*, 21(2), 395–409.
- Fossen, T.I. (2000). Nonlinear passive control and observer design for ships. *Modeling, Identification and Control*, 21(3), 129–184.
- Fossen, T.I. (2011). *Handbook of Marine Craft Hydrodynamics and Motion Control*. Wiley.
- Fossen, T.I. and Pettersen, K.Y. (2014). On uniform semiglobal exponential stability (USGES) of proportional line-of-sight guidance laws. *Automatica*, 50(11), 2912–2917.
- Fossen, T.I. and Strand, J.P. (1999). Tutorial on nonlinear backstepping: Applications to ship control. *Modeling, Identification and Control*, 20(2), 83–135.
- Khalil, H.K. (2002). *Nonlinear Systems*. Prentice Hall.
- Lamnabhi-Lagarrigue, F., Panteley, E., Lefeber, E., and Loria, A. (2005). *Advanced Topics in Control Systems Theory: Lecture Notes from FAP 2004*. Springer.
- Pavlov, A., Nordahl, H., and Breivik, M. (2009). MPC-based optimal path following for underactuated vessels. *in Proceedings of the 8th IFAC Conference on Manoeuvring and Control of Marine Craft, Guarujá, Brazil*.
- Refsnes, J.E., Sørensen, A.J., and Pettersen, K.Y. (2008). Model-based output feedback control of slender-body underactuated AUVs: Theory and experiments. *IEEE Transactions on Control Systems Technology*, 16(5), 930–946.
- Sandved, F. (2015). *Remote Control and Automatic Path-following for C/S Enterprise I and ROV Neptunus*. MSc thesis. Dept. of Marine Technology, Norwegian University of Science and Technology, Trondheim, Norway.
- Skejic, R., Breivik, M., and Berg, T.E. (2011). Investigating ship maneuvers around a floating structure under the influence of a uniform current in deep and calm water. *in Proceedings of the 2nd International Conference on Ship Manoeuvring in Shallow and Confined Water: Ship to Ship Interaction, Trondheim, Norway*.
- Sørensen, M.E.N. and Breivik, M. (2015). Comparing nonlinear adaptive motion controllers for marine surface vessels. *in Proceedings of the 10th IFAC Conference on Manoeuvring and Control of Marine Craft, Copenhagen, Denmark*.

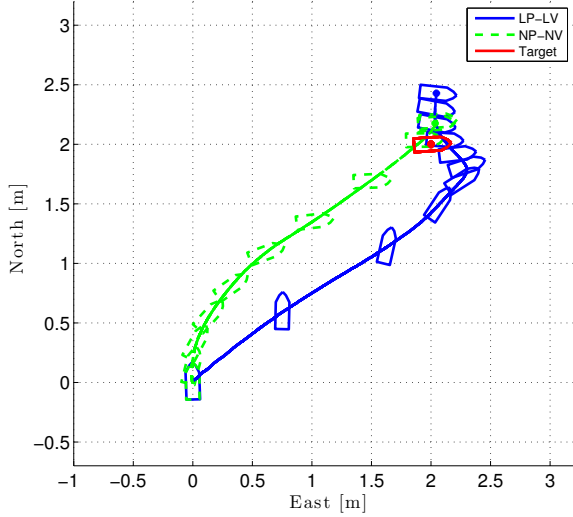


Fig. 12. Experiment: Vessel point stabilisation

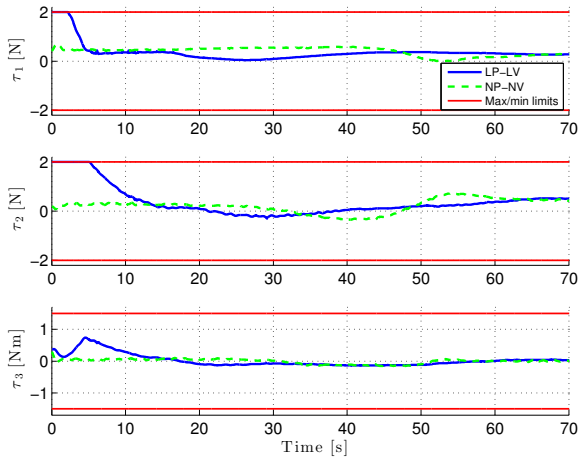


Fig. 13. Experiment: The commanded control inputs and force/moment saturation limits

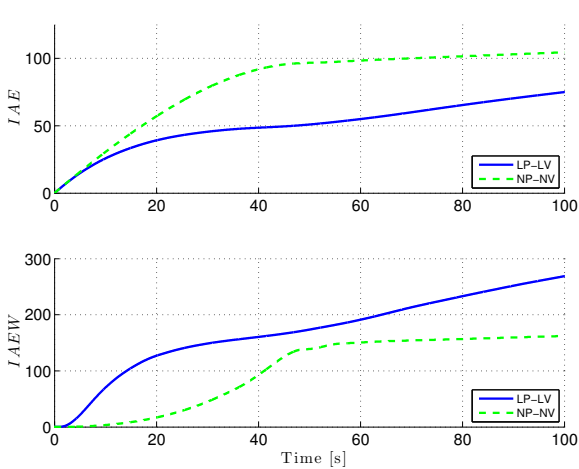


Fig. 14. Experiment: IAE and IAEW performance metrics

rate saturation in addition to magnitude saturation, and thus investigate the effect of time-varying Δ_i -parameters.